ADVANCED CLOUDS, AEROSOLS AND WATER VAPOUR PRODUCTS FOR SENTINEL-3/OLCI

Retrieval of Cloud Top Pressure from MERIS and OLCI O2 A-Band Measurements

Algorithm Theoretical Basis Document (ATBD)
and
Input/Output Data Definition (IODD)

Issue 1.1, 10.10.2015

ESRIN/Contract No: 4000111860/14/I-NB

prepared by
Jürgen Fischer and Rene Preusker

Document, Version	Date	Changes	Originator
ATBD, v1.0_draft	20.01.2015	Original	Jürgen Fischer, Rene Preusker
ATBD v1.0	20.07.2015	Original	Jürgen Fischer, Rene Preusker
ATBD v1.1	9.10.2015	• Added section information content OLCI • Minor changes	Jürgen Fischer, Rene Preusker

Table of Content

Acronyms and Abbreviations

AATSR	Advanced Along Track Scanning Radiometer
AERONET	AErosol RObotic NETwork
AOD	Aerosol Optical Depth
ANN	Artificial neural network
ATBD	Algorithm Theoretical Basis Document
BC	Brockmann Consult
BEAM	Basic Envisat Tool for AATSR & MERIS (http://envisat.esa.int /services/beam/)
CALIPSO-CALIOP	Cloud-Aerosol Lidar with Orthogonal Polarization, part of A-train
CloudSat	Cloud Satellite part of A-train
CNES	Centre National d'Etudes Spatiales
COT	Cloud optical thickness
CTP	Cloud-top pressure
DJF	Design justification file
DPM	Detailed Processing Model
DQWG	Data quality working group
DUE	ESA Data User Element programme (http://due.esrin.esa.int/)
Δz	Geometrical thickness
ECSS	European Co-operation for Space Standardisation (documents available at ESTEC at the Requirements and Standards Division)
Envisat	ESA satellite (see http://envisat.esa.int/)
EO	Earth Observation
EOS	Earth Observing System / NASA
ESA	European Space Agency (http://www.esa.it/export/esaCP/index.html)
ESTEC	European Space Research and Technology Centre
ESRIN	European Space Research Institute (http://www.esa.it/export/esaCP/index)
FUB	Free University Berlin
FoV	Field of View
GCOS	Global Climate Observing System
GEWEX	Global Energy and Water Exchanges Project
GPS	Global Positioning System
GUAN	GCOS Upper Air Network
GVaP	GEWEX Global Water Vapor Project
HITRAN	High-resolution transmission molecular absorption database
HOAPS	Hamburg Ocean Atmosphere Parameters and Fluxes from Satellite
ICAP	International Cooperative for Aerosol Prediction (ICAP)
IODD	Input Output Data Definition Doc.
ISCCP	GEWEX International Satellite Cloud Climatology Project
L1/L2	Level 1 / Level 2
LBL	Line-by-line
LUT	Look-up table
MERIS	Medium Resolution Imaging Spectrometer Instrument (http://envisat.esa.int/)
MODIS	Moderate Resolution Imaging Spectroradiometer (on board the NASA EOS-Aqua satellite)
MOMO	Matrix Operator Modell
MSG	METEOSAT Second Generation
MWR	Microwave Radiometer
NASA	National Aeronautics and Space Administration
OCO-2	Orbiting Carbon Observatory - 2
OE	Optimal estimation
OLCI	Ocean and Land Colour Instrument on board Sentinel-3
PARASOL	Polarization & Anisotropy of Reflectances for Atmospheric Sciences mission
PDF	Portable Document Format
POLDER	Polarization and Directionality of the Earth's Reflectances
PVR	Product Validation and evolution Report
QA4EO	Quality Assurance framework for Earth Observation
RB	Requirements baseline
RTC / RTM	Radiative Transfer Code / Model
RR	Reduced Resolution
SCIAMACHY	Scanning Imaging Absorption Spectrometer for Atmospheric Cartography
SEOM	ESA Scientific Exploitation of Operational Missions Element

	programme (http://seom.esa.int/)
SOS	Successive Order of Scattering
SoW	Statement of Work
TCWV	Total Column Water Vapour
TOA	Top of atmosphere

References

Applicable Documents

[AD-1]	EOP-GMQ, 2014: *SEOM S3-CAWA: advanced Clouds, Aerosols and WAter vapour products for Sentinel-3/OLCI, Statement of Work*. GMES-GSEG-EOPG-SW-13-0047, iss. 1 rev0, dated 14.01.2014 (https://earth.esa.int/web/sppa/activities/cawa/projects-documents/)
[AD-2]	Fox, N. et al., 2010: *A guide to establishing validated models, algorithms and software to underpin the Quality Assurance requirements of GEO* (http://www.qa4eo.org/docs/QA4EO-QAEO-GEN-DQK-002_v4.0.pdf)
[AD-3]	Eaton et al. , 2011: *NetCDF Climate and Forecast (CF) Metadata Convention* (http://cf-pcmdi.llnl.gov/)
[AD-4]	Fischer, J. et al. 2015: *CAWA – Requirement Baseline Document* (https://earth.esa.int/web/sppa/activities/cawa/projects-documents/)

Reference Documents

[RD-1]	*MERIS Cloud-Top Pressure Algorithm Theoretical Basis Document - ATBD 2.3 (https://earth.esa.int/instruments/meris/atbd/atbd_2.3.pdf)*
[RD-2]	Hollmann et al. (2013) The ESA Climate Change Initiative: Satellite Data Records for Essential Climate Variables ESA Climate Change Initiative. Bull. Amer. Meteor. Soc., 94, 1541–1552.
[RD-3]	GCOS, 2010: Implementation Plan for the Global Observing System for Climate in Support of the UNFCCC (2010 update, November 2009).
[RD-4]	GCOS, 2011: Systematic observation requirements for satellite-based data produced for climate, 2011 updates. GCOS -154 Global Climate Observing System, 2011. http://www.wmo.int/pages/prog/gcos/Publications/gcos-154.pdf

1 Introduction

1.1 Purpose

This document provides information about the physical background, technical structure and the functional principle of the CAWA cloud top pressure retrieval as defined with the SEOM S3 'advanced Clouds, Aerosols and WAter vapour products for Sentinel-3/OLCI' CAWA project, which aims to the development and improvement of advanced atmospheric retrieval algorithms for the Envisat/MERIS and Sentinel-3/OLCI mission.

1.2 Structure of the document

This document addresses the *Algorithm Theoretical Baseline* (ATBD) and the *Input/Output Data Definition* (IODD). It is structured as following:

- Overview of the retrieval algorithm scheme (Chapter 2)
- Description of the forward operator (Chapter 3)
- Input Output Data Definition (Chapter 4)
- Assumptions and limitations (Chapter 5)
- Conclusions (Chapter 6).

1.3 Satellite instruments

The measurements of the satellite sensors MERIS and OLCI used in this study are briefly described in the following.

1.3.1 MERIS and OLCI

The key mission objective for the Sentinel-3 OLCI instrument is the continuity of the ENVISAT MERIS instrument capability. The primary mission of OLCI is the observation of the spectral distribution of upwelling radiance just above the sea surface (the water-leaving radiance) that is then used to estimate a number of geophysical parameters through the application of specific bio-optical algorithms. Atmospheric correction for ocean colour data is challenging (International Ocean Colour Coordinating Group - IOCCG, 2010) as only about 4% of the radiation measured by a satellite instrument originates from the water surface and sensors require high signal to noise ratio (SNR), particularly for the 'blue' bands (Donlon et al, 2012). This requires an accurate retrieval and description of the atmospheric state with respect to scattering and absorption processes. This points to the secondary objective, the detection of atmospheric properties, which include cloud detection (pixel classification) and aerosol detection, which is important not only for atmospheric correction but also for the monitoring of air-pollution.

The S-3 OLCI instrument is based on the opto-mechanical and imaging design of ENVISAT MERIS (see Table 1). The instrument is a quasi-autonomous, self contained, visible push-broom imaging spectrometer and incorporates the following significant improvements when compared to MERIS:

- An increase in the number of spectral bands (from 15 to 21),
- Improved SNR and a 14-bit analogue to digital converter,
- Improved long-term radiometric stability,
- Mitigation of sun-glint contamination by tilting cameras in westerly direction by 12.6°,
- Complete coverage over both land and ocean at 300 m Full-Resolution (FR),
- Improved instrument characterization including stray light, camera overlap, and calibration diffusers.

The cameras are arranged to slightly overlap with each other to cover a wide 68.5° across-track field of view as shown in Figure 1. The OLCI swath is not centred at nadir (as in the MERIS design) but is

tilted 12.6° westwards to mitigate the negative impact of sun-glint contamination that affects almost half of the MERIS observations at sub-tropical latitudes.

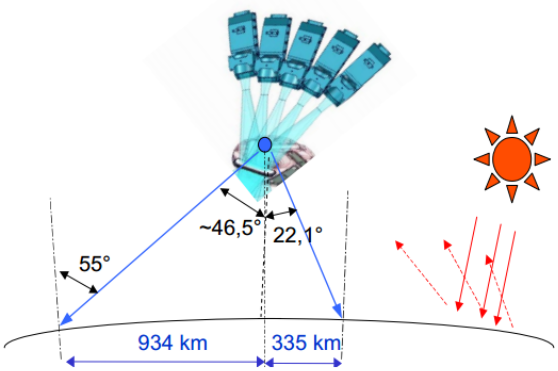

Figure 1: OLCI features a tilted field of view to avoid sun-glint

OLCI bands are optimised to measure ocean colour over the open ocean and coastal zones. A new channel at 1.02µm has been included to improve atmospheric and aerosol correction capabilities, additional channels in the O2A spectral region are included for improved cloud top pressure (height) and water vapour retrieval, and a channel at 673nm has been added for improved chlorophyll fluorescence measurement. In principle, the OLCI programmable acquisition design allows spectral bands to be redefined in both location and width during commissioning of the instrument after which time they will be fixed for the mission duration.

Table 1: The spectral bands of OLCI and MERIS.

OLCI Band	Center [nm]	Width [nm]
Oa1	400	15
Oa2	412,5	10
Oa3	442,5	10
Oa4	490	10
Oa5	510	10
Oa6	560	10
Oa7	620	10
Oa8	665	10
Oa9	673,75	7,5
Oa10	681,25	7,5
Oa11	708,75	10
Oa12	753,75	7,5
Oa13	761,25	2,5
Oa14	764,375	3,75
Oa15	767,5	2,5
Oa16	778,75	15
Oa17	865	20
Oa18	885	10
Oa19	900	10
Oa20	940	20
Oa21	1020	40

MERIS Band	Center [nm]	Width [nm]
Me1	412,5	10
Me2	442,5	10
Me3	490	10
Me4	510	10
Me5	560	10
Me6	620	50
Me7	670	15
Me8	681,25	10
Me9	708,75	10
Me10	753,75	10
Me11	761,875	3,75
Me12	778,75	15
Me13	865	10
Me14	885	10
Me15	900	10

1.3.2 CloudSat and Caliop

In 2006 the first space-born aerosol and cloud radar and lidar instruments, the Cloud Profiling Radar (CPR) CloudSat (Stephens et al., 2002) and CALIOP (Cloud-Aerosol Lidar with Orthogonal Polarization) onboard CALIPSO (Cloud-Aerosol Lidar and Infrared Pathfinder Satellite Observations) (Winker et al.,

2003) have been launched. Both satellite missions are part of the Afternoon Train (A-train) satellite constellation and have complemented the established observations by providing observations on the vertical structure of aerosols and clouds. A synergistic product of the cloud-radar and the lidar provides the vertical cloud profile, which is also reliable for thin cirrus (Mace and Zhang, 2014).

This product and the MODIS Mb1 observations are used to find a relationship between the horizontal texture and their vertical cloud profiles.

1.3.3 OCO-2

The OCO-2 instrument provides high spectral resolution in three spectral bands ranging from 0.758µm µm to 0.772µm, from 1.594µm to 1.620µm and from 2.040 to 2.080µm. OCO-2 is also part of the A-train.

Due to the tilting capacity of the OCO-2 instrument, the measuring conditions along the OLCI swath can be simulated. The OCO-2 observations are taken to relate multi-spectral O2 A-band observations to vertical cloud profiles, which provide valuable measurements for validation.

2 Cloud top pressure retrieval - Overview

The approach of satellite-borne O_2 *A* band-based cloud-top pressure measurements is illustrated in *Figure 2*. The sunlight reaching the cloud-top is backscattered and a part finally reaches the sensor on board a satellite. For a well mixed atmospheric gas like oxygen and a known vertical profile of the pressure and the temperature the traversed air mass can be estimated by radiance measurements within an absorption band. For monochromatic light in a non-scattering atmosphere the relation between the amount of absorption and the traversed air mass can be described by Lamberts law.

However, this simple approach is not sufficient because it neither includes scattering of radiation inside and outside the cloud nor correctly describes the absorption of non-monochromatic light. The impact of microphysical cloud properties, varying cloud optical thickness, surface albedo as well as the observation geometry on the radiances have been investigated by radiative transfer simulations. For the development and definition of a cloud-top pressure algorithm the use of radiative transfer models is of advantage for a systematic analysis of the influence of cloud and surface properties as well as of the influence of measurement errors.

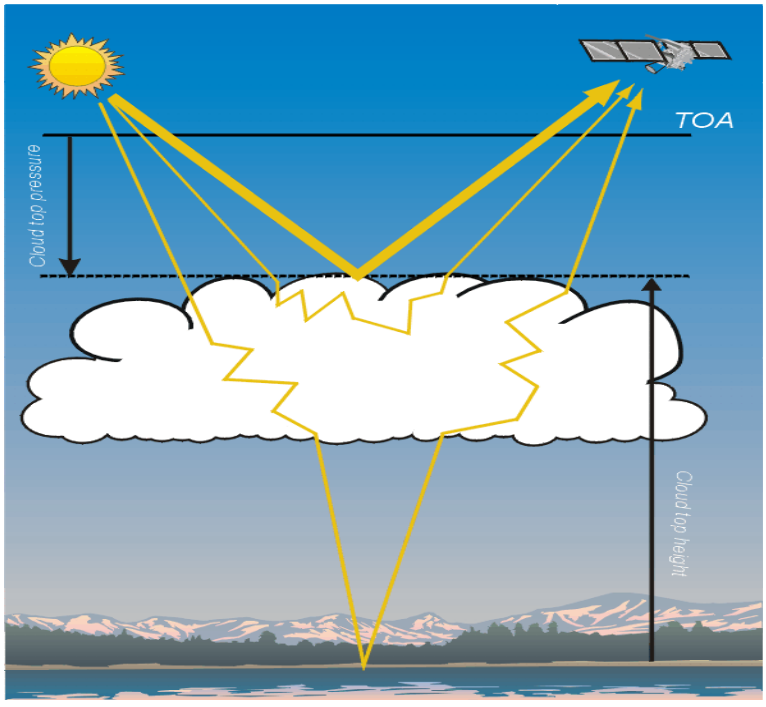

Figure 2: Illustration of the principle of the cloud-top pressure detection using absorption

of solar radiation due to well-mixed atmospheric gases.

Since no simple relationship or analytical formulation of the coherence between the radiances at top of atmosphere and cloud-top pressure exists, radiative transfer simulations are used to establish an appropriate algorithm. There are different mathematical methods to solve the inverse problem. An approach, based on a complete radiative transfer code is not efficient enough with respect to computation time (Kollewe and Fischer, 1994). Faster semi-empirical radiative transfer codes have deficits with respect to accuracy. Several methods provide a solution:

- A polynomial approach such as proposed by Fischer and Graßl (1991) would reduce the size of the required database and the computation times by fitting the dependence between radiances and cloud parameters by polynomials. The coefficients are determined with multi-linear regression methods from the results of radiative transfer simulations.
- Neural networks are able to reduce the size of the required database and the computation times drastically. Matrices derived from a supervised learning procedure using simulation results, relate a vector of input information to a vector of cloud properties of interest. They are able to account for the non-linear correlation of the multi spectral radiances, cloud properties and cloud-top pressures (Preusker et al, 2007). However, the main drawback is that measuring errors and atmospheric constrains are difficult to introduce in the retrieval process.
- A 1-D-var approach has been shown to be most successful in the retrieval of atmospheric properties and their further use in numerical weather prediction models (Rogers, 2000). The use of instantaneous radiative transfer simulations or Look-up Tables depends on the application and, of course, on the layout of the retrieval scheme. The advantage of LUTs is the high performance with respect to computational resources and the potential use of complex radiative transfer codes.

3 Algorithm description

3.1 Problem Understanding

The utilisation of spectral measurements within the oxygen absorption bands for observations of the earth and atmosphere from space started in the early sixties. There has been an early interest in monitoring the cloud top pressure and other geophysical properties from upcoming new space borne instruments. Those ideas attracted considerable attention both in the United States and in Soviet Union from the 1960s until the early 1980s. Due to manifold problems in instrumentation and radiative transfer modelling, the interpretation of the measured signals failed. Nevertheless, a steady progress has been realised due to improvements in radiative transfer modelling, in providing more precise data of the O_2 absorption line parameters and of instrumentation (Fischer and Grassl, 1991; Fischer et al., 1991; Preusker et al., 2007).

The most important parts in a radiative transfer code, suitable to simulate the radiative transfer processes in the O_2 A-band as required for this study, are the description of the interaction of scattering and absorption processes, the adequate formulation of the gaseous absorption in the vertical structure of the atmosphere, and the incorporation of the instrumental characteristics. This points to a critical review of the commonly used HITRAN database, even though it has undergone several revisions including the oxygen line-by-line parameters during the last decade (Rothman et al, 2012). To address the vertical structure of the atmosphere more correctly than before, recent improvements in the formulation of the atmospheric transmission have been considered to overcome significant uncertainties in the estimation of the absorption coefficients (Bennartz and Fischer, 2001; Doppler et al., 2013). There are a number of radiative transfer codes which are in principle applicable to simulate TOA radiance within the Oxygen A band (Fischer and Grassl, 1991; Heidinger and Stephens, 2000; Hasekamp and Butz, 2008; Kolemeijer et al., 2001). However, the combination of the different requirements will drive the selection of a suitable RTM for this study.

The radiative transfer model MOMO, based on a matrix operator method, has been designed for a coupled atmosphere-ocean system including rough water or anisotropic land surfaces and simulates the complete Stokes vector for any given spectral and vertical resolution (Hollstein and Fischer, 2011).

The actual cloud-top pressure retrieval from ENVISAT/MERIS measurements, as implemented in the ESA ground segment, is based on MOMO simulations, which are used to define an artificial neural net (Fischer et al., 2012).

An early inter-instrument comparisons with AATSR, MISR, and MODIS, both are on-board Terra, point to an overestimation of the MERIS cloud-top pressure for high clouds (Naud et al., 2004), but Lindstrot et al. (2006) have demonstrated in an aircraft campaign, that the MERIS estimated cloud-top pressures for low-level clouds agree well with simultaneously taken LIDAR observations. Within ESA's cloud-cci activities, Carbajal-Henken et al. (2012, 2014) demonstrated that the overestimation of the cloud top pressure of high clouds is due to the insufficient knowledge of the vertical profile of the cloud properties and thus originates in an inaccurate modelling of the photon path length within the cloud.

The main problem in the cloud top pressure retrieval using the O2 A-band is the photon penetration into the clouds as already discussed in Fischer and Grassl (1991) and Preusker and Lindstrot (2010). The fact that MERIS has only one O2 A-band channel limits the potential to retrieve direct information on the vertical cloud structure. There is a significant improvement in the cloud-top pressure expected by introducing cloud-types, which are characterised by their vertical LWC/IWC profiles.

The retrieval of cloud properties from MERIS is focused on the cloud amount, cloud top pressure and to some extend to cloud optical thickness. MERIS provides no observations beyond 1 µm, which excludes observations of cloud liquid or ice water or cloud top temperatures. A strong benefit of MERIS for cloud observation is the O2 A-band channel, which has been used to derive cloud top pressure. As discussed above, MERIS observes boundary layer clouds with high accuracy, but fails when optically thin cloud layers are on top. Lindstrot et al. (2010) studied multilayer clouds by the combination of MERIS and AATSR observations and found that both, the O2 A-band and the thermal infrared measurements, contribute to a more accurate cloud top pressure retrieval for vertically structured clouds. Those findings motivated Carbajal-Henken et al. (2012, 2014) to develop a 1D-Var approach for a cloud properties retrieval. When the vertical cloud profile, as measured by CloudSat is taken considered into the retrieval of the MERIS cloud top pressure the agreement is surprisingly good with the active radar measurements (see Figure 3). Within the thin upper layers, the photons penetrate quite deeply in the cloud and the retrieval misses to detect the cloud top. The O2 A-band of MERIS is not sensitive enough to detect clouds with optically thickness below 0.5. The upper layer clouds in the tropics and mid-latitudes consist usually of optically thin clouds, which would require additional high spectral measurements in the O2 A-band for their detection.

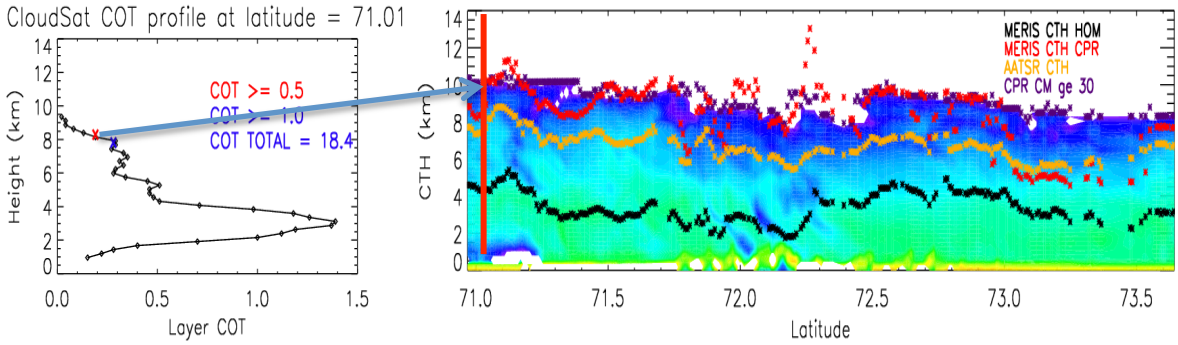

Figure 3: Cloud optical thickness, derived from the satellite cloud radar CloudSat (left panel); Cloud top pressures derived from MERIS (Ground-segment), from MERIS with vertical cloud profile information, from AATSR and CloudSat, the optical colours represent the cloud optical thickness (right panel) (Carbajal-Henken et al., 2012).

The challenge for the cloud top pressure algorithm is to account for high-level thin cloud layers and vertical structure of the cloud optical thickness. This might be tackled by the introduction of cloud types, which are related to distinct cloud profiles. We expect that the new MERIS CTP product will benefit from the introduction of cloud-types with more realistic cloud extinction profiles and an uncertainty estimate.

The challenge for the next generation O2 A-band based CTP retrieval is the efficient use of the three OLCI O2 A-band channels to account more realistically for the penetration depth of the photon into the clouds.

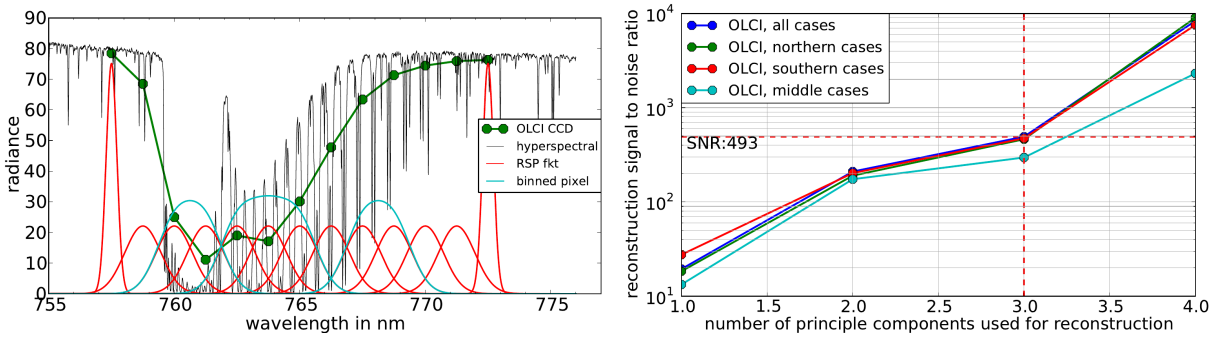

Figure 4: Radiance measurements of the TANSO-FTS on board GOSAT (black lines) and OLCI response function (red) (left panel); Number of principle components used for the reconstruction of TANSO-FTS measurements and related signal-to-noise ratio (right panel).

The potential of O2 A-band measurements has been studied by means of an independent information analysis. Therefore we simulated the potential OLCI channels around the O2 A-band by measurements of the TANSO-Fourier-Transform-Spectrometer on board the Japanese GOSAT satellite, which provides radiances with spectral resolutions of 0.01 nm. The reflected nadir radiances are taken along a polar orbit. The spectrally high-resolution data are binned to build individual OLCI channels (see Figure 4). The reference channels are assumed to be free of atmospheric absorption features with a reduced response function. Two years of observations are used to invest the information content of potential OLCI O2 A-band measurements above clouds, however, knowing that only a rigid cloud-mask has been applied. A separation in observation of the northern and southern hemisphere and the tropics give some hints for interpretation of the findings (see Figure 4, right panel). The reconstruction of the full TFS observed spectra could be achieved with 3 independent pieces for the northern and southern hemispheric clouds. Above the tropics the complex cloud systems effect more independent information, expressed in a reduced signal-to-noise ratio where already 3 pieces are sufficient to construct the full observed spectra. The lower the required signal-to-noise ratio to observe 3 independent pieces of information, the more information is delivered by O2 A-band observations. Following these results we expect a significant increase in the accuracy of OLCI cloud-top pressure product, when the retrieval algorithm is able to account for the radiation transfer processes within the oxygen absorption of a cloudy atmosphere.

In summary of this investigation we conclude, that OLCI's O2 A-band channels carry three independent pieces of information, which can be detected with the sensors SNR characteristic. The measurements carry a fourth piece of independent information, which might be more complicated to retrieve, since the variations caused by it are beyond a signal to noise level of 500. It is to mention that this study is based purely on measurements, but the variability in the GOSAT dataset might be lees pronounced due to larger spatial resolution compared to the OLCI spatial resolution of 260 by 300 m^2. Therefore this study provides a lower bound for the information carried by future OLCI measurements.

3.2 Theoretical description

The extinction of radiation due to gaseous absorption depends on the absorber mass and on the absorption coefficients within the radiation path. The measured radiance decreases if the photon path within the atmosphere increases. Therefore, the relation between radiances within and outside absorption bands contains information on the absorber mass penetrated by the photons. For a well-mixed absorbing gas like oxygen, the total absorption is linear with the total photon path length. The appearance and the position of clouds alter the possible path lengths significantly. Figure 5 shows simulated radiances in the wavelength domain of the O_2 A-band for different cloud-top pressures. In both figures the enhanced absorption for lower cloud-top pressures is clearly shown. For a sun zenith angle $\theta_S=0^\circ$ and nadir view, there is only a minor dependency of window radiances on cloud-top pressure (Figure 5, left). For higher sun zenith angles the effects of aerosol and Rayleigh scattering increase and thus lower intensities in window channels for lower cloud-top heights (Figure 5, right).

The vertical profile of a cloud affects the radiances within and outside the oxygen absorption band differently. While radiances in window channels only depend on total optical thickness, radiances within the absorption band are also related to the vertical distribution of liquid water. Photons penetrating into deeper cloud layers have a higher probability of becoming absorbed. In Figure 6 the ratio of simulated radiances at λ=761.875nm and λ=753.75nm is shown in a polar plot and a principal plane representation. The left and right side of the Figure 6 belong to the same cloud optical properties and cloud-top pressure but they differ in geometrical thickness of the clouds (Δz=1km and 4km). The ratio of radiances at λ=760nm and λ=753.75nm is smaller for clouds with a larger geometrical thickness because the photons penetrate into deeper cloud layers.

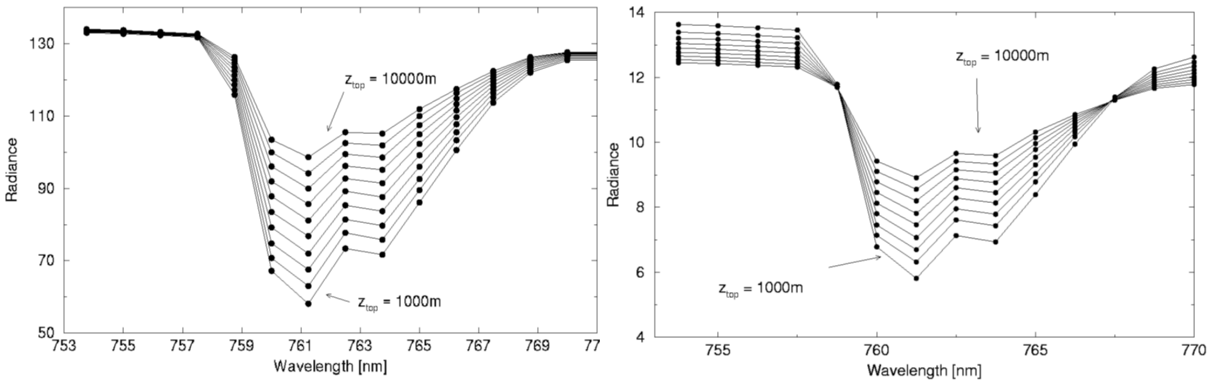

Figure 5: Simulated radiances in the O_2 A-band with different cloud-top pressures. Calculations for solar zenith angle ϑ_0=0° (upper) and solar zenith angle ϑ_0=82.15° (lower) and for the cloud parameters: optical thickness δ_c=25, geometrical thickness Δz=1000m and effective radius r_e=8µm. Radiance values in W/m²sr^{-1}µm^{-1}.

The information on the penetration depth is required for precise cloud-top pressure retrieval. The penetration depth can be taken into account by using additional measurements within the absorption band (Fischer and Grassl, 1991). Depending on the wavelength the absorption in the O_2 A-band differs and the radiation penetrates to different depths within the cloud. During the ESA ELAC '90 aircraft campaign 160.000 multi-spectral radiance measurements within the O_2 A-band were taken with a spectral resolution of 0.4nm above different types of clouds over Europe (Fischer and Kollewe, 1994). According to a multi-variate analysis three independent quantities for the cloud-top pressure retrieval could be identified, which are related to three channels, two within and one outside the absorption band. The photon penetration was found to be the most challenging process to account for and to predict within the retrieval scheme. The vertical distribution and the size of the cloud droplets, expressed by the liquid water content have to be considered within the algorithm. For typical clouds the liquid water content increases with height above the cloud base until a maximum in the upper half is reached (Pruppacher, 1980). Also, the liquid water content of different

cloud types such as stratus, stratocumulus and cumulonimbus differ only by a factor of two as long as the temperature does not exceed 280K (Feigelson, 1984). According to this, the variation of liquid water content and its vertical distribution is limited. LWC profiles for different cloud types have to be considered for the development of the cloud-top pressure algorithm.

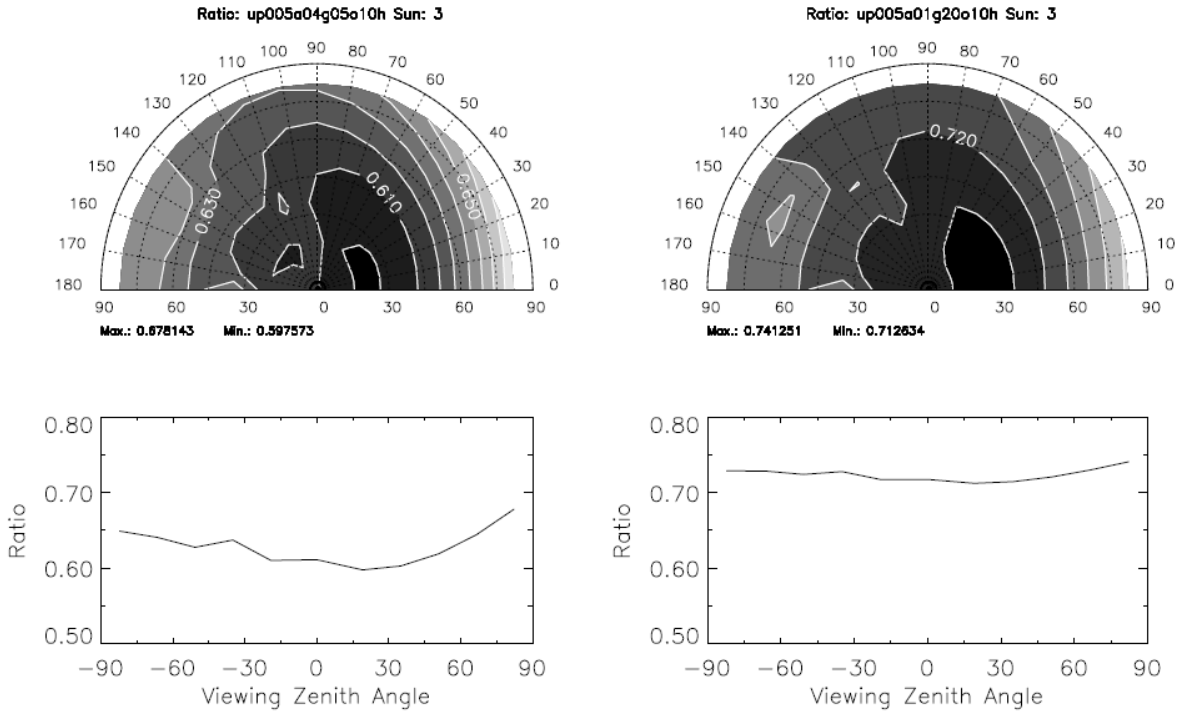

Figure 6: Polar plot and principle plane graph of the simulated field of the ratio between radiances in the O2 A-band at λ =761.875nm (bandwidth $\Delta\lambda$=1.25 nm) and in the window channel at λ =753.75nm. Calculations are done for solar zenith angle θ_S=35° and for cloud parameters: optical thickness τ_c=20, cloud-top height z_{top}=10km and effective radius r_{eff}=8µm. The geometrical thickness is Δz=4km (left) and Δz=1km (right).

In a sensitivity study performed by Preusker and Lindstrot (2009), the sensitivity of the ratio of the MERIS absorption channel 11 (761.875nm) and window channel 10 (753.75nm) to a set of varying cloud, atmospheric and surface parameters was studied: cloud top pressure, cloud optical thickness, cloud geometrical thickness, cloud fraction, atmospheric temperature profiles, surface albedo, surface pressure. It was shown that the sensitivity of the MERIS ratio to changes in cloud top pressure is significant except for a thin cloud above a highly reflecting surface. Furthermore, the sensitivities to changes CTP and geometrical thickness are strongly correlated, making it difficult to disentangle them. Changes in cloud microphysics and the temperature profile only have minor impacts with maximum errors of less then 10 and 20hPa, respectively, and are considered small with regards to other error sources.

The largest source of error in the CTP retrieval is the presence of multi-layer clouds, in the study defined as thin cirrus over low-level water clouds. Multi-layer clouds represent an extreme case of inhomogeneous cloud vertical profiles.

3.3 Universal forward operator

It is understood that the retrieval of cloud top pressure from MERIS- and OLCI-type O2 A-band measurements has to be based on reference channels at 753.75nm and 778.75nm, the O2 A-band channels at 761.875nm and 761,25nm, 764.375nm, 767.5nm, respectively, as well as on external data from NWP services. Accurate radiative transfer simulations of all MERIS and OLCI bands are

based on input data such as the surface reflectivity spectrum, the surface pressure, the atmospheric temperature profile and the vertical profile of the cloud micro-optical and micro-physical properties. While all mentioned parameters are crucial for the radiative transfer simulations, some can easily be obtained from operational NWP services while others must be retrieved from MERIS/OLCI measurements.

In the given context, surface and atmospheric parameters should be included from NWP data, which leaves the cloud parameters open for the retrieval. The exact vertical profile of effective radius and cloud optical thickness are not accessible from the two/three MERIS or even the four/five channels of OLCI and must effectively be reduced to a parameter state with only few degrees of freedom. The cloud effective radius and its distribution have only minor impacts on the used channels, but should be considered in a quantitative approach.

It is feasible to use CloudSat vertical cloud profiles and total cloud optical thickness from AATSR or SLSTR to reduce the dimensionality of the problem to effective values for cloud optical thickness, cloud droplet effective radius, and cloud top height. This reduction procedure is not unique and basically expresses a set of prior assumptions about the vertical profile of clouds. While this reduction of dimensionality enables retrievals in the first place, it is also the main uncertainty source for the retrieval of CTP. Possible errors are then mainly driven by the differences of the assumed and real cloud vertical profile, which also included effects of multi-layer clouds.

Depending on the used approach for inverse modelling, we introduce external knowledge and associated uncertainties into the retrieval to improve the overall retrieval accuracies. In the framework of optimal estimation (following Rodgers 2000) this is achieved by including an initial guess together with an expected error estimate. A CTP retrieval based on the two or four channels would greatly benefit from an accurate prior on cloud optical thickness and cloud effective radius. Due to the high spatio-temporal variability of cloud fields, such information is of best use if the OLCI cloud optical thickness product is used. A strong advantage of the optimal estimation framework is, that the retrieval is also attempted without an accurate prior, but at the cost of increased uncertainty of the retrieval product.

The temperature profile of the atmosphere can affect the retrieval of CTP, especially for optical thin clouds. Similar as for the cloud vertical profiles, the representation of vertical profiles with sufficient accuracy is a challenge in a LUT based approach. It is usually not feasible to express the total possible variability of a profile, i.e. independent values in each layer, as independent parameters in a LUT, since the sheer size of these tables grows very rapidly with an increasing number of parameters. This problem is mitigated by using similar dimensionality reduction techniques as for the cloud vertical profiles. Lindstrot and Preusker (2012) expressed profiles by a model with only a few parameters or a separation strategy.

Since the MERIS / OLCI instrument uses multiple cameras to cover the swath of 1150 km/1350 km, the spectral characterisation of each camera and its consideration within the retrieval process is essential (Lindstrot et al, 2011). This is included in the radiative transfer simulations to reduce systematic model errors. One way of including this effect is to perform the radiative transfer simulations on a hyper-spectral grid with sufficient oversampling of the expected response functions. Such an approach increases the computational cost of generating the LUT, but offers at the same time a clear path to an instrumental independent retrieval scheme, where the same LUTs and retrieval schemes is consistently applied to MERIS and OLCI. The size of the hyper-spectral LUTs is controlled via an approach introduced by Hollstein and Lindstrot (2014).

3.3.1 Cloud classification pre-processor

Since the spectral measurements of MERIS and OLCI and their corresponding information content are limited, we introduced a procedure to account for the vertical profile of cloud extinction. As discussed in Carbajal et al. (2012) the vertical cloud profiles have been related to cloud types, characterised by the satellite measurements of CloudSat and MERIS/AATSR. Within a stand-alone MERIS/OLCI approach, we suffer from observations beyond λ>1050nm. Therefore we use the spatial heterogeneity of clouds for a characterisation and an estimate of their vertical profiles.

A relationship between the spatial heterogeneity of clouds and their vertical profiles is established by the use of MODIS (band Md1 at λ=645nm, Δx=250m) and CloudSat (vertical cloud profile) measurements (Mace and Zhang, 2014). The texture parameters are the mean, homogeneity and entropy, calculated from a sub-matrix of 5x5 elements (pixels) as described in Schroeder et al. (2002).

Standardized vertical cloud profiles, derived from CloudSat, are selected via the derived texture parameters and used in the further cloud top pressure retrieval process.

3.3.2 MERIS processor

The MERIS processor is based on Look-up Tables containing used input data and the resulting radiances of all used MERIS bands and the corresponding spectral characterisation.

The simulations where performed using the Matrix Operator Model (MOMO, Hollstein and Fischer, 2012). The radiances were calculated for different solar zenith angles (SZA), viewing zenith angles (VZA), relative azimuth angles (RAA), surface reflectances, cloud optical thicknesses and vertical profiles related to a selection of cloud types.

Water surfaces are simulated with a fixed wind speed of v=7m/s taken the Cox and Munk (1954) wave slope distribution into account. Above land surfaces a Lambertian reflector is assumed with reflectance values between α=0.0 and α=0.95 in steps of $\Delta\alpha$=0.05. The vertical cloud structure is estimated by the derived cloud type (3.3.1).

All data are stored in LUTs. The parameter dimensions of the LUTs are regularly spaced, allowing a fast indexing and interpolation for the forward operator. The N-dimensional interpolation of X* in an regular parameter space $[p_1, p_2, \ldots, p_N]$ is divided into the following two steps:

1. Normalization of the input variables:

$$p_i^* = \frac{p_i - p_i^l}{p_i^u - p_i^l}$$

   where p^l and p^u is the nearest lower and nearest upper parameter entry in the Look-up Table.

2. Interpolation by a weighted sum of the 2^N enveloping neighbours in the Look-up Table:

$$\begin{aligned} X^*(p_1, p_2, \ldots, p_N) = {} & (1-p_1^*)(1-p_2^*)\ldots(1-p_N^*)X^{l,l,\ldots,l} \\ & + (0-p_1^*)(1-p_2^*)\ldots(1-p_N^*)X^{u,l,\ldots,l} \\ & + \cdots \\ & + (0-p_1^*)(0-p_2^*)\ldots(0-p_N^*)X^{u,u,\ldots,u} \end{aligned}$$

3.3.3 OLCI processor

The OLCI processor is primarily based on the MERIS processor, but using the three O2 A-band channels, which provide more information on the vertical cloud profile. The differences between the MERIS and OLCI procedures are described in the section below.

3.4 Retrieval scheme

This retrieval scheme derives *CTP* values with the help of an inverse modelling technique. Deviations between modelled and measured radiances within the O2 A-band absorption are iteratively reduced by changing the cloud top pressure. In order to include information from all absorption bands and to account for the measurement error in the inversion scheme, the inversion technique presented in Sect. 3.3.1 is used. The uncertainty estimate is derived after the last retrieval step, by taking into account all error influences. The individual retrieval steps are described in the following sections.

3.4.1 Inversion technique

The state vector, which has to be found in the iterative optimization routine includes: The cloud top pressure CTP and an expression for the vertical cloud properties profile. Starting with the first guess, CTP is adapted by minimizing the differences between simulated and measured radiances. The CTP value for the next iteration step is derived by the following scheme after (Rodgers, 2000):

$$G = (K_i^T S_e^{-1} K_i)^{-1} (K_i^T S_e^{-1}) \quad (8)$$

$$X_{i+1} = X_i + (G(y - F_i)) \quad (9)$$

where K_i is the Jacobian matrix of the iteration step *i*, that contains the partial derivatives of the radiance to the CTP and COT(z) values in each band, S_e the measurement error covariance matrix which contains the measured radiance scaled with the signal to noise ratio (SNR) for each band. *y* contains the measured and F_i the modelled radiances, whereby F_i is defined as following

for MERIS:

$$F_i = F_i(CTP, COT\,; ext[z], \alpha, \theta_s, \theta_v, \phi_v) \quad (10)$$

and for OLCI

$$F_i = F_i(CTP, COT, \Delta z; ext[z], \alpha, \theta_s, \theta_v, \phi_v) \quad (11)$$

with surface albedo α, solar zenith distance θ_s, viewing zenith θ_v and azimuth ϕ_v, vertical cloud extinction and the retrieved cloud properties from MERIS *CTP* and *COT*. OLCI's additional O2 A-band measurements provide also information on the geometrical thickness and thus directly on the vertical cloud profile.

If in future a reliable *a-priory* knowledge about the state *X* is available, the gain *G* in the iteration (equation 8 and 9) can be adapted accordingly (Rodgers, 2000).

3.4.2 Uncertainty estimate

After the iteration procedure the retrieval uncertainty is calculated, taking into account the following sources of uncertainty:

- residual model error
- instrument uncertainty (SNR)
- uncertainty due to the missing information of the vertical cloud properties profile.
- uncertainty due to the cloud micro-physics, expressed by effective radius of the cloud droplets
- uncertainty due to the missing information about the true temperature profile
- uncertainty due to the estimation of the surface reflectance

For the error quantification, these model parameter uncertainties assembled in the error covariance matrix S_b are propagated into the measurement space using the standard error propagation and added to the measurement error covariance matrix S_e:

$$S_y = S_e + K_b^T S_b K_b \quad (11)$$

where K_b is the parameter Jacobian. The resulting error covariance matrix S_y is then propagated into the state vector space using the Jacobian *K* that is the partial derivative of the modelled radiance with respect to CTP for each band. The resulting error covariance matrix *S* is a direct measure of uncertainty in CTP space [Rogers, 2000]:

$$\hat{S}^{-1} = K^T S_y^{-1} K \quad (12)$$

In the following, it is described, how the individual error sources are estimated. As outlined before, the CTP is affected most by the vertical cloud profile, the cloud optical thickness and the surface reflectance. For each of these parameters a perturbed CTP is calculated from the Look-up Tables, by perturbing the input accordingly. There is no information available about the vertical cloud profile. Consequently, a *CTP** is calculated presuming a cloud layer with a thickness of 1000 m. Additionally, a *CTP** is taken from the LUTs supposing another cloud geometrical thickness. These *CTP** are used to derive perturbed TOA-radiances L^*_{TOA}. Finally, the difference $(\Delta L)^2 = (L_{TOA} - L^*_{TOA})^2$ is added to the measurement error variance S_e.

The error due to differences between the simulation- and the real cloud profile is evaluated by comparing the CTP derived from a real example taken from a CloudSat profile to CTP using the standard cloud profiles. To estimate the uncertainty due to the surface background information, the surface pressure was perturbed by 20hPa and subsequently committed to the transmittance forward operator. Again, $(\Delta L)^2$ is calculated and added to S_e.

The uncertainties of the surface reflectance range from 1% to 5%. Similar to the approach pictured above, a perturbed TOA radiance is calculated and the resulting deviation is contributed to S_e. Finally the residual model error, that is the difference between measurement and modelled radiance from the last iteration step is added to the measurement covariance matrix that consists of the sensor noise.

4 Input Output Data

This section defines the input data, required for the processing of MERIS and OLCI data as well as the output of the MERIS and OLCI cloud processor.
The CTP processor is using normalised radiances. The observation geometry is expressed in viewing zenith angle, Sun zenith angle and azimuth difference angle, which are all given in the L1b product-files (see Table 3a).

Table 3a: Satellite measurements taken from the Level 1b instrument data files.

Quantity	Unit	Valid range	Source	Comment
Normalized radiance	1/sr	0 -1	L1b	Depending on instrument different bands serve as absorption and as window bands (see Section 1.3)
Viewing zenith angle	deg	0-60	L1b	
Sun zenith angle	deg	0-75	L1b	
Azimuth difference angle	deg	0-180	L1b	

The auxiliary data used in the CTP processor are taken for MERIS and OLCI from ESA's meteorology data-files provided by ECWMF, and additional accessible data on surface albedo and aerosols, i.e. from ESA/NASA archive. For MODIS the ERA-interim data are used.

Table 3b: Auxiliary data used in the CTP processor and it's valid range.

Quantity	Unit	Valid range	Source	Comment
Surface pressure	hPa	200 - 1050	QNH from ECMWF, adapted to actual surface height	GFS is also possible
Surface albedo	1	0 – 0.95	ESA	
Surface temperature	K	260-330	ECMWF	

Aerosol optical thickness	1	0-1.0	Ideally GRASP, or MODIS 8-day average	If no available, climatology can be used (0.1)
Aerosol optical thickness uncertainty	1		Taken from GRASP or MODIS, resp.	

The output of the CTP processor is the cloud top pressure and it's uncertainty in hPa. For further analysis of the convergence of the inversion process, the estimated transmission and the number of required iterations are given (see Table 4).

Table 4: Output of the CTP algorithm after applying to the Level 1b instrument data files; CTP and it's estimated uncertainty, convergence as a logical expression, intermediate results to check the inversion process.

Quantity	Unit	Valid range	Resolution	Accuracy	Comment
CTP	hPa	0 - 1020	TBD	TBD	
CTP uncertainty	hPa		TBD	TBD	
COT	1	0 - 254	TBD	TBD	
COT uncertainty	1		TBD	TBD	
Cloud type	1	TBD	TBD	TBD	
Convergence	Logical				
Intermediate results, i.e. first guess, transmission, number of iterations					Can be used for debugging purpose

The processor is divided into two main units. One unit is responsible for all input/output operations; the other unit is retrieving the CTP for a single pixel. The communication between both units is performed using files, pipes or streams in JSON. This allows the easy exchange of modules for testing and developing. The operational IO part is BEAM. The CTP part is written in python and FORTRAN.

5 Assumptions and limitations

Generally, the quality of the CTP retrieval algorithm strongly depends on the reliability of the cloud mask and the used vertical cloud profile. For example MERIS does not provide measurements in the thermal infrared, the screening of optically thin cirrus clouds is difficult, but will be processed. The CTP retrieval of OLCI will be significantly enhanced compared to MERIS by using all three O2 A-band channels.

6 Conclusions

A new retrieval method has been defined and developed to estimate CTP from satellite measurements, using O_2 A-band measurements. The 1D-Var algorithm is based on a fast forward operator, which accounts for cloud type, cloud top pressure, and cloud optical thickness. The algorithms for MERIS and OLCI are consistent and based on the same principles and procedures. A realistic uncertainty estimate is given on a pixel-by-pixel basis where the uncertainties of measurement and forward model are considered respectively.

It is intended to use the spatial inhomogeneity to discriminate different cloud types, which correspond to characteristic cloud vertical profiles. Those vertical profiles are input for the retrieval

of cloud top pressure for MERIS and OLCI. However, due to additional channels within the O2 A–band absorption of OLCI with respect to MERIS, the retrieval accuracy increases.

Validation of the CTP, COT and cloud type products is challenging due to the limit of simultaneous Caliop (Lidar) and CloudSat (cloud radar) measurements, as provided by NASA's A-train. Those measurements are rare and limited to the northern and southern parts of the Earth due to the orbits of Envisat and Sentinel-3, which does not fit well with the orbit of the A-train. The upcoming Earthcare mission, which also provides active cloud radar and lidar measurements, will also fly in an orbit with limited overlap to Sentinel-3 observations.

7 References

Bennartz, R. and J. Fischer, 2000: A modified k-distribution approach applied to narrow band water vapour and oxygen absorption estimates in the near infrared. Journal of Quantitative Spectroscopy & Radiative Transfer, 66:539–553, Sept. 2000.

Bennartz, R. and R. Preusker, 2006: Representation of the photon path-length distribution in a cloudy atmosphere using finite elements. Journal of Quantitative Spectroscopy and Radiative Transfer, Volume 98.

Carbajal-Henken, C., R. Lindstrot, F. Filipitsch, A. Walther, J. Fischer, 2012: FAME-C: Retrieval of Cloud Top Pressure with Vertically Inhomogeneous Cloud Profiles, Proc. International Radiation Symposium 2012, Berlin, Germany, 06-10 August 2012.

Carbajal-Henken, C., Lindstrot, R., Preusker, R., and Fischer, J., 2014: FAME-C: cloud property retrieval using synergistic AATSR and MERIS observations. Atmos. Meas. Tech. Discuss., 7, 4909-4947, doi:10.5194/amtd-7-4909-2014.

Clough, S. A. , M. W. Shephard, E. J. Mlawer, J. S. Delamere, M. J. Iacono, K. Cady-Pereira, S. Boukabara, and P. D. Brown, 2005: Atmospheric radiative transfer modeling: a summary of the AER codes. Journal of Quantitative Spectroscopy & Radiative Transfer, 91:233–244, Mar. 2005.

Delwart S., R. Preusker, L. Bourg, R. Santer, D. Ramon, J. Fischer, 2006: MERIS in flight spectral calibration. Int. J. Remote Sensing, 28, 479-496.

Doppler, L., R. Preusker, R. Bennartz, J. Fischer, 2013: k-bin and k-IR: k-distribution methods without correlation approximation for non-fixed instrument response function and extension to the thermal infrared. Journal of Quantitative Spectroscopy and Radiative Transfer, 09 / 2013.

Fischer, J. and H. Grassl, 1984: Radiative transfer in an atmosphere-ocean system: an azimuthally dependent matrix-operator approach. Applied Optics, 23:1032–1039, Apr. 1984.

GCOS, 2006: Systematic Observation Requirements for Satellite-based Products for Climate - Supplemental details to the satellite-based component of the Implementation Plan for the Global Observing System for Climate in Support of the UNFCCC (GCOS-107, WMO/TD. No 1338, September 2006).

GCOS, 2010: Implementation Plan for the Global Observing System for Climate in Support of the UNFCCC (2010 update, November 2009).

GCOS, 2011: Systematic observation requirements for satellite-based data produced for climate, 2011 updates. GCOS -154 Global Climate Observing System, 2011. http://www.wmo.int/pages/prog/gcos/Publications/gcos-154.pdf

Hollstein, A. and J. Fischer, 2012: Radiative transfer solutions for coupled atmosphere ocean systems using the matrix operator technique. Journal of Quantitative Spectroscopy and Radiative Transfer Volume 113, Issue 7, May 2012, Pages 536–548.

Hollstein, A. and Lindstrot, R.: Fast reconstruction of hyperspectral radiative transfer simulations by using small spectral subsets: application to the oxygen A band, Atmos. Meas. Tech., 7, 599-607, doi: 10.5194/amt-7-599-2014, 2014.

Lindstrot, R., R. Preusker, Th. Ruhtz, B. Heese, M. Wiegner, C. Lindemann, and J. Fischer, 2006: Validation of MERIS cloud top pressure using airborne lidar measurements, J. Appl. Meteor. Clim. , 45 (12), 1612-1621.

Lindstrot, R, R. Preusker and J. Fischer, 2009: The retrieval of land surface pressure from MERIS measurements in the oxygen A band. J. Atmos. Oceanic Technol., 26 (7), 1367–1377.

Lindstrot, R, R. Preusker and J. Fischer, 2010: The empirical correction of stray light in the MERIS oxygen A band channel. Journal of Atmospheric and Oceanic Technology, 27, 1185-1194.

Lindstrot, R. and Preusker, R., 2012: On the efficient treatment of temperature profiles for the estimation of atmospheric transmittance under scattering conditions, Atmos. Meas. Tech., 5, 2525–2535, doi:10.5194/amt-5-2525-2012.

Naud, C, J.-P. Muller, B. Baum, R. Bennarzt, R. Frey, P. Menzel, H. Zhang, J. Fischer, R. Preusker, 2004: Inter-comparison of MERIS, MODIS and MISR cloud top heights. In: European Space Agency, (Special Publication) ESA SP (pp. 19 - 24).

Preusker, R., and R. Lindstrot, 2009: Remote Sensing of Cloud-Top Pressure Using Moderately Resolved Measurement within the Oxygen A Band—A Sensitivity Study. J. Applied Meteoro. Climatology, 48, 1564-1574.

Mace, G. G., and Q. Zhang, 2014: The CloudSat radar-lidar geometrical profile product (RL-GeoProf): Updates, improvements, and selected results. J. Geophys. Res. Atmos., 119, 9441–9462, doi:10.1002/2013JD021374.

McClatchey, R., R. Fenn, J. Selby, F. Volz, and J. Garing, 1972: Optical properties of the atmosphere (3rd ed.). Technical report, Air Force Cambridge Research Laboratories, 1972.

Rodgers, C., 2000: Inverse Methods for Atmospheric Sounding: Theory and Practice. World Scientific Pub Co., 2000.

Rothman, L. S. , C. P. Rinsland, A. Goldman, S. T. Massie, D. P. Edwards, J.-M. Flaud, A. Perrin, C. Camy-Peyret, V. Dana, J.-Y. Mandin, J. Schroeder, A. Mc- Cann, R. R. Gamache, R. B. Wattson, K. Yoshino, K. Chance, K. Jucks, L. R. Brown, V. Nemtchinov, and P. Varanasi. Reprint of: The HITRAN molecular spectroscopic database and HAWKS (HITRAN Atmospheric Workstation): 1996 edition. Journal of Quantitative Spectroscopy & Radiative Transfer, 111:1568– 1613, Aug 2010.

Schröder, M., R. Bennartz, L. Schüller, R. Preusker, P. Albert and J. Fischer, 2002: Generating cloudmasks in spatial high-resolution observations of clouds using texture and radiance information. Int. J. Remote Sensing, 23, 4247-4261.

Wiscombe, W. J., 1980: Improved Mie scattering algorithms. Applied Optics, 19:1505– 1509, May 1980.